Scattering Performance of Log-Periodic Dipole Array

Kei Yokokawa, Keisuke Konno, *Member, IEEE*, and Qiang Chen, *Senior Member, IEEE*

***Abstract*—In this letter, the scattering performance of a log-periodic dipole array (LPDA) is numerically and experimentally demonstrated. Radiation and scattering performance of the LPDA is shown. Numerical simulations clarify that a 3-dB bandwidth of an LPDA scatterer becomes narrow due to the distortion of its RCS pattern. Relation between the total length and bandwidth performance of the LPDA scatterer is numerically examined to extend its narrow bandwidth. The optimized LPDA scatterer achieves the bandwidth of 1:1.8. The optimized LPDA scatterer is fabricated, and the measured scattering performance is shown to confirm the numerical results.**

***Index Terms*—Log-periodic dipole array (LPDA), scattering, wideband.**

I. Introduction

IN PREVIOUS studies, the radiation performance of various ultrawideband antennas, such as bowtie antennas [1], tapered slot antennas [2], spiral antennas [3], and log-periodic dipole array (LPDA) antennas [4], [5], has been demonstrated. These ultrawideband antennas have been studied, and their radiation performance is well known. However, the scattering performance of these ultrawideband antennas has not been clarified sufficiently. For example, the scattering performance of reflectarrays using the spiral-shaped microstrip patch element was only reported [6]. The scattering performance of structure of the LPDA that is well known as an ultrawideband antenna has not been discussed. On the other hand, 3-D scatterers have received much attention due to the recent advance of 3-D printing technologies [7]–[9]. Although various scatterers can be fabricated easily using 3-D printing technologies, the technologies have not been applied to fabricating the LPDA.

In this letter, the scattering performance of the LPDA is reported quantitatively. Scattering performance of the LPDA is numerically obtained and compared to its radiation performance. Moreover, the optimum total length of the LPDA is obtained to extend the 3-dB bandwidth of the LPDA. Finally, the optimized LPDA is fabricated using a 3-D printing technology, and its scattering performance is measured to confirm the numerical performance. The designed LPDA is expected to be a wideband array element for wideband FSSs or reflectarrays.

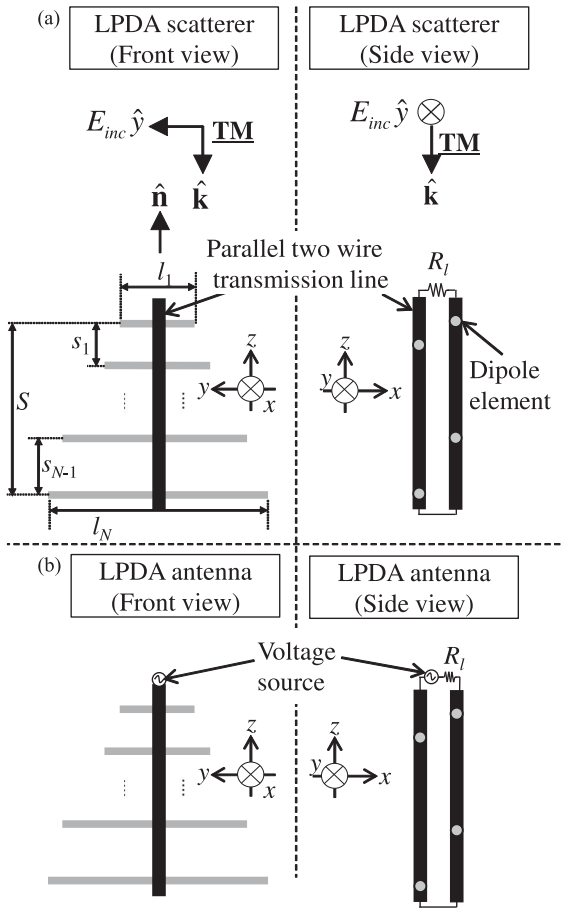

Fig. 1. (a) LPDA scatterer excited by the TM plane wave. (b) LPDA antenna excited by a voltage source.

II. Principle and Structure of the LPDA

The geometry of the LPDA scatterer and the LPDA antenna is shown in Fig. 1. In Fig. 1, k_0 is the wavenumber of free space, and $E_{\rm inc}$ is the amplitude of the TM plane wave. The LPDA consists of a parallel two-wire transmission line connecting with dipole elements. For calculating scattering performance, the LPDA scatterer is excited by the TM plane wave, while the LPDA antenna is excited by a voltage source for calculating its radiation performance.

The LPDA is designed as in following three steps. At first, the length l_1 of the shortest dipole element that corresponds to the highest operating frequency and the length l_N of the

Manuscript received March 26, 2016; revised May 31, 2016 and July 9, 2016; accepted August 13, 2016. Date of publication August 17, 2016; date of current version April 3, 2017. This work was supported in part by JSPS KAKENHI under Grant 26820137, JSPS Postdoctoral Fellowships for Research Abroad, and computational resources of the HPCI system provided by Cyberscience Center, Tohoku University, through the HPCI System Research Project (Project ID:hp140052).

K. Yokokawa is with the Mitsubishi Electric Corporation, Tokyo 100-8310, Japan (e-mail: Yokokawa.Kei@bc.MitsubishiElectric.co.jp).

K. Konno and Q. Chen are with the Department of Communications Engineering, Tohoku University, Sendai 980-8579, Japan (e-mail: konno@ecei.tohoku.ac.jp; chenq@ecei.tohoku.ac.jp).

Color versions of one or more of the figures in this letter are available online at http://ieeexplore.ieee.org.

Digital Object Identifier 10.1109/LAWP.2016.2601244

longest dipole element that corresponds to the lowest operating frequency are determined, where N is the number of total dipole elements in the LPDA. The structure bandwidth of the LPDA B_s can be then defined as follows:

$$B_s = \frac{l_N}{l_1}. \tag{1}$$

Next, the scale factor τ of the LPDA is defined. Both the length l_n of the nth dipole element and spacing s_n between the nth and (n+1)th dipole elements are recursively calculated using τ, l_{n-1}, and s_n, as follows:

$$\tau = \frac{l_{n-1}}{l_n} = \frac{s_{n-1}}{s_n} \qquad \text{where n = 1, 2, ..., N.} \tag{2}$$

After the structure bandwidth B_s and the scale factor τ are defined, the total number of dipole elements N can be determined as

$$N = \left[1.5 + \frac{\log B_s}{\log \frac{1}{\tau}}\right] \tag{3}$$

where square brackets [ ] show the gauss symbol and $[x]$ indicates the largest integer that is less than or equal to x (e.g., $[1.3] = 1$, $[3.8] = 3$).

The radiation performance of the LPDA antenna is well known. For example, it is known that the operating bandwidth B of the LPDA antenna approaches the structure bandwidth B_s when the spacing s_n becomes smaller [10]. However, in general, the operating bandwidth depends not only on its structure but also on its excitation. Therefore, it must be examined whether the LPDA scatterer shows wideband scattering performance or not. In this letter, the bandwidth of the scattering performance is defined as the 3-dB bandwidth of the radar cross section (RCS). The wideband scattering performance means that the bandwidth of the LPDA is larger than 20%.

III. Simulation Results

A. Radiation and Scattering Performance

The LPDA scatterer and the LPDA antenna, whose structure bandwidth is from 4 to 12 GHz, were designed. The performance of the designed LPDA was simulated using the method of moments (MoM). The simulated radiation performance and scattering performance of the LPDA are shown in Figs. 2 and 3, respectively. The radiation performance of the LPDA antenna was evaluated using actual gain, while the scattering performance of the LPDA scatterer was evaluated using the RCS.

As shown in Fig. 2, it is found that 3-dB bandwidth of the LPDA antenna is 1:2.3. It is also seen that the actual gain of the LPDA antenna is almost constant in the designed structure bandwidth. On the other hand, as shown in Fig. 3, the RCS of the LPDA scatterer oscillates sharply in the designed structure bandwidth. As a result, 3-dB bandwidth of the LPDA scatterer is 1:1.5. Therefore, it can be said that the 3-dB bandwidth of the LPDA scatterer is narrower than that of the LPDA antenna. In order to clarify the mechanism of the oscillation of the RCS, both the RCS pattern and radiation pattern at 3.8, 5.4, and 7 GHz are obtained as shown in Figs. 4 and 5. The RCS

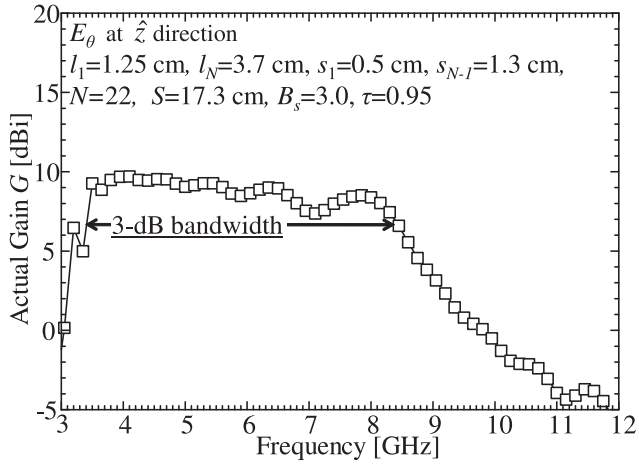

Fig. 2. Radiation performance of the LPDA antenna (E_θ on yz-plane, z-direction).

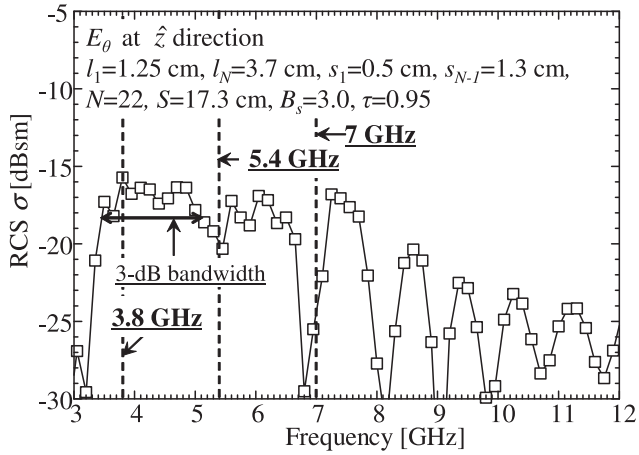

Fig. 3. Scattering performance of the LPDA scatterer (E_θ on yz-plane, z-direction).

patterns of the LPDA scatterer are distorted at 5.4 and 7 GHz, while the mainlobe of the LPDA antenna is clearly directed to its endfire direction at three frequencies. Difference between RCS patterns and radiation patterns is caused by the difference of the current distribution between the LPDA excited by different sources. The LPDA antenna is excited by a voltage source loaded with the end of the parallel two-wire transmission line. As a result, the dipole elements in the LPDA antenna are excited via the parallel two-wire transmission line. On the other hand, dipole elements in the LPDA scatterer are excited directly by a plane wave. Resultant difference of current distribution between the LPDA antenna and scatterer leads to the difference of radiation and RCS patterns. Therefore, the structure of the LPDA scatterer should be optimized in order to reduce the distortion of the beam and extend its bandwidth.

B. Optimization of Bandwidth

Bandwidth of the LPDA scatterer is affected by its dimensions, such as τ and the total length S of the LPDA scatterer,

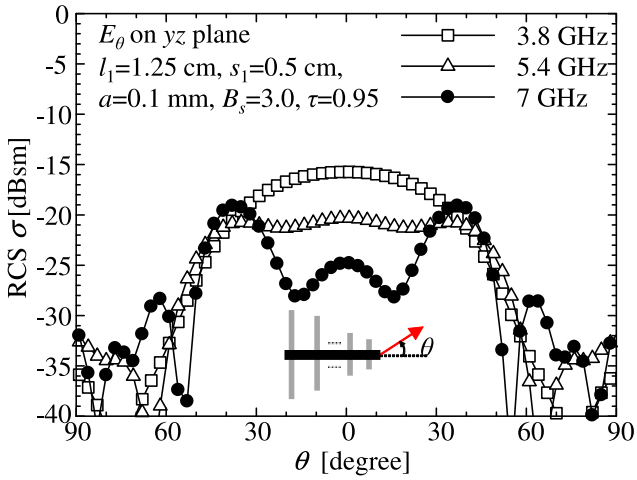

Fig. 4. RCS pattern of the LPDA scatterer.

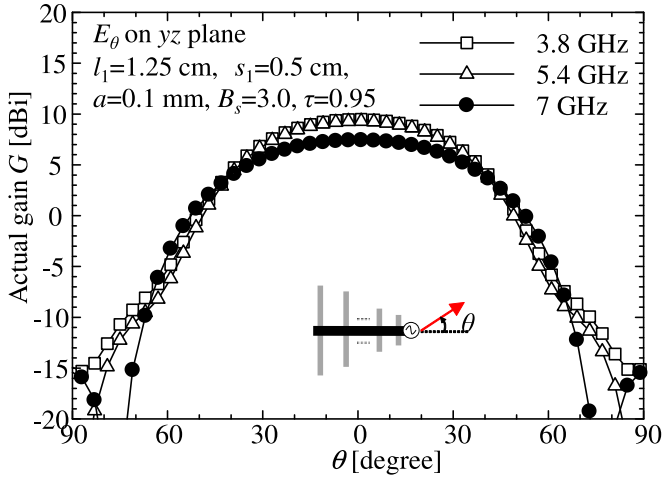

Fig. 5. Radiation pattern of the LPDA antenna.

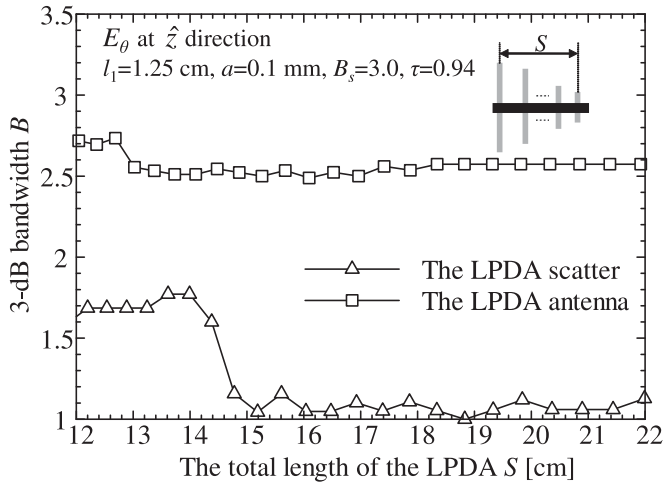

Fig. 6. Effect of S on 3-dB bandwidth B.

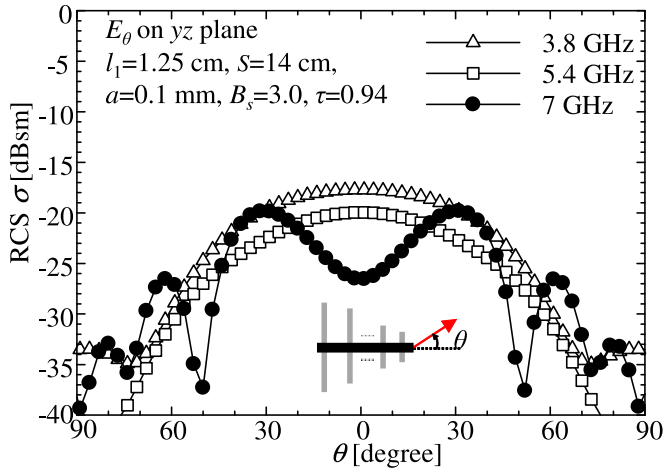

Fig. 7. RCS pattern of the optimized LPDA scatterer.

which is defined as

$$S = \sum_{n=1}^{N-1} s_n . \tag{4}$$

For example, τ should be given carefully in order to improve the bandwidth of the LPDA scatterer. As shown in (2), the length of each dipole element varies smoothly as τ approaches to 1. Therefore, the bandwidth of the LPDA scatterer is expected to be enhanced as τ approaches to 1. Such relationship between τ and the bandwidth of the LPDA scatterer is easily found. Finally, as expected, the maximum bandwidth of the LPDA scatterer is achieved at $\tau = 0.94 \sim 0.95$ as a result of numerical simulations for various combinations of τ and S. Therefore, in this section, the total length S of the LPDA, which strongly affects the bandwidth of the LPDA scatterer, is mainly discussed.

The 3-dB bandwidth of the LPDA scatterer and the LPDA antenna is shown as a function of S in Fig. 6. From Fig. 6, it can be seen that the operating bandwidth of the LPDA scatterer is strongly affected by S, while that of the LPDA antenna is less affected by S. Fig. 6 also shows that the 3-dB bandwidth of the LPDA scatterer decreases when S is relatively long. The degradation is assumed to be caused by the phase difference between the current of dipole elements excited by TM plane wave directly and that coupled via the parallel two-wire transmission line. Therefore, it is concluded that the total length S (and τ) of the LPDA scatterer should be optimized in order to minimize the phase difference. The RCS pattern of the optimized LPDA scatterer with $S = 14$ cm is shown in Fig. 7. The bandwidth of the LPDA scatterer with $S = 14$ cm is maximized. It is clarified that the distortion of the RCS pattern at 5.4 GHz is improved compared to Fig. 4. The distortion of the RCS pattern at 7 GHz is not improved yet because the phase of scattering field of each dipole element on the LPDA is still not in-phase at z-direction.

IV. Fabrication and Measurement

In this section, measurement results of the scattering performance of the LPDA scatterer are shown. A photograph of a fabricated LPDA scatterer is shown in Fig. 8. The LPDA scatterer was fabricated using 3-D printing technology (Dimension BST768 with 0.254-mm precision) and consists of ABS (Acrylonitrile butadiene styrene) resin coated by conductive ink

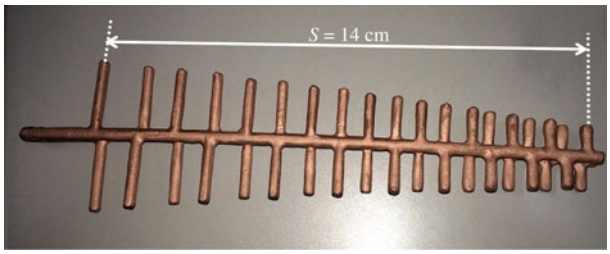

Fig. 8. Photograph of the fabricated LPDA scatterer.

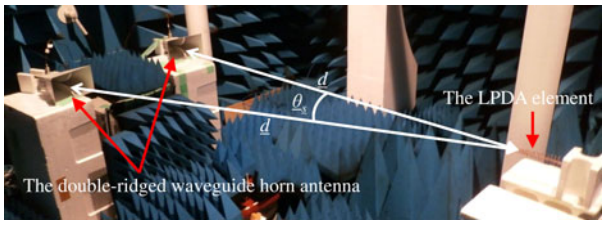

Fig. 9. Photograph of measurement in anechoic chamber.

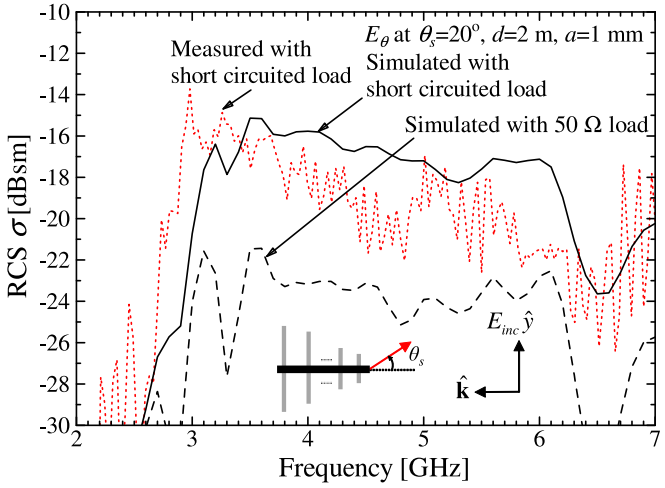

Fig. 10. Measurement and simulation result of the LPDA scatterer.

made of copper (S-SHIELD EMI-21, measured conductivity $\sigma \approx 2 \times 10^4$ S/m at 4 GHz). The conductive ink was sprayed on the fabricated LPDA. Conductivity of the ink was obtained from a measured transmission coefficient of a microstrip line fabricated in the same manner. Both ends of the fabricated LPDA scatterer are short-circuited, and a 50-Ω resistance is not loaded because the termination of the fabricated LPDA scatterer is mechanically difficult. The geometry of the LPDA scatterer is the same as the optimized one, except for the termination. Fig. 9 shows the system for measuring RCS of the LPDA scatterer in a radio anechoic chamber. It was difficult to measure the backscattering signal using a monostatic measurement system due to the poor dynamic range of the measurement system. Therefore, we selected a bistatic measurement system. Transmitting and receiving antennas were BBHA 9120D double-ridged waveguide horn antennas from SCHWARZBECK Mess Elektronik.

The measured RCS is shown in Fig. 10. As a reference, the RCS obtained by numerical simulation is plotted in the same figure. The conductivity obtained from measurement was included in the RCS simulation. It is found that the measured RCS agrees well with the simulated RCS except for a ripple and a little frequency shift. Therefore, it can be said that the scattering performance of the LPDA scatterer is verified experimentally. The ripple and the frequency shift in the measured RCS pattern come from the surface roughness of the fabricated LPDA and the error of the measurement system. On the other hand, it is found that 5 dB loss is roughly introduced in the simulated RCS when the LPDA scatterer is terminated by the 50-Ω resistance. It can be said that the LPDA scatterer should be short-circuited in order to keep a large value of the RCS. Due to the limitation of our measurement system, measurement of the RCS pattern of the LPDA scatterer is difficult, and the results will be obtained in the future.

V. Conclusion

The scattering performance of the LPDA was studied. Numerical simulation clarified that the bandwidth of the LPDA scatterer can be narrow due to the distortion of the RCS pattern. Therefore, the total length of the LPDA scatterer must be optimized to improve the distortion of the RCS pattern. The bandwidth of the LPDA scatterer is strongly affected by the total length of the LPDA scatterer. The RCS of fabricated LPDA scatterer shows agreement with simulated RCS except for a little frequency shift.

Acknowledgment

The authors would like to thank the staff of the Cyberscience Center, Tohoku University.

References

[1] A.C. Durgun, C.A. Balanis, C.R. Birtcher, and D.R. Allee, "Design, simulation, fabrication and testing of flexible bow-tie antennas," *IEEE Trans. Antennas Propag.*, vol. 59, no. 12, pp. 4425–4435, Dec. 2011.

[2] L. Pazin and Y. Leviatan, "A compact 60-GHz tapered slot antenna printed on LCP substrate for WPAN applications," *IEEE Antennas Wireless Propag. Lett.*, vol. 9, pp. 272–275, 2010.

[3] N. Rahman and M.N. Afsar, "A novel modified Archimedean polygonal spiral antenna," *IEEE Trans. Antennas Propag.*, vol. 61, no. 1, pp. 54–61, Jan. 2013.

[4] G. Zhai, Y. Cheng, Q. Yin, S. Zhu, and J. Gao, "Gain enhancement of printed log-periodic dipole array antenna using director cell," *IEEE Trans. Antennas Propag.*, vol. 62, no. 11, pp. 5915–5919, Nov. 2014.

[5] J. Mruk, Z. Hongyu, M. Uhm, Y. Saito, and D. Filipovic, "Wideband mm-wave log-periodic antennas," in *Proc. Eur. Conf. Antennas Propag.*, Mar. 2009, pp. 2584–2587.

[6] S. Datthanasombat *et al.*, "Spiral microstrip patch element for reflectarrays," in *Proc. IEEE Int. Symp. Antennas Propag.*, Jul. 2001, vol. 3, pp. 721–724.

[7] P. Nayeri *et al.*, "3D printed dielectric reflectarrays: Low-cost high-gain antennas at sub-millimeter waves," *IEEE Trans. Antennas Propag.*, vol. 62, no. 4, pp. 2000-2008, Apr. 2014.

[8] B. S.-Izquierdo and E.A. Parker, "3-D printing of elements in frequency selective arrays," *IEEE Trans. Antennas Propag.*, vol. 62, no. 12, pp. 6060–6066, Dec. 2014.

[9] S.N. Azemi and W.S.T. Rowe, "Development and analysis of 3D frequency selective surfaces," in *Proc. Asia Pacific Microw. Conf.*, Dec. 2011, pp. 693–696.

[10] R. Carrel, "The design of log-periodic dipole antennas," in *Proc. IRE Int. Conv. Rec.*, vol. 9, pp. 61–75, Mar. 1966.